

Article

Resistance Characteristics of SMA Actuator Based on the Variable Speed Phase Transformation Constitutive Model

Yifan Lu ¹ , Rongru Zhang ¹, Ye Xu ¹, Lei Wang ^{2,*} and Honghao Yue ^{1,*}

¹ State Key Laboratory of Robotics and System, Harbin Institute of Technology, Harbin 150001, China; yf.lu@hit.edu.cn (Y.L.); 18S008186@stu.hit.edu.cn (R.Z.); xuyehit@163.com (Y.X.)

² School of Naval Architecture and Ocean Engineering, Harbin Institute of Technology, Weihai 264200, China

* Correspondence: leonwl@hit.edu.cn (L.W.); block@hit.edu.cn (H.Y.)

Received: 10 March 2020; Accepted: 23 March 2020; Published: 24 March 2020



Abstract: The shape memory alloy (SMA)-based actuators have been increasingly used in different domains, such as automotive, aerospace, robotic and biomedical applications, for their unique properties. However, the precision control of such SMA-based actuators is still a problem. Most traditional control methods use the force/displacement signals of the actuator as feedback signals, which may increase the volume and weight of the entire system due to the additional force/displacement sensors. The resistance of the SMA, as an inherent property of the actuator, is a dependent variable which varies in accordance with its macroscopic strain or stress. It can be obtained by the voltage and the current imposed on the SMA with no additional measuring devices. Therefore, using the resistance of the SMA as feedback in the closed-loop control is quite promising for lightweight SMA-driven systems. This paper investigates the resistance characteristics of the SMA actuator in its actuation process. Three factors, i.e., the resistivity, the length, and the cross-sectional area, which affect the change of resistance were analyzed. The mechanical and electrical parameters of SMA were obtained using experiments. Numerical simulations were performed by using the resistance characteristic model. The simulation results reveal the change rules of the resistance corresponding to the strain of SMA and demonstrate the possibility of using the resistance for feedback control of SMA.

Keywords: shape memory alloy; phase transformation; constitutive model; resistance characteristics

1. Introduction

The shape memory alloy (SMA) is a kind of alloy which can remember its original shape. When deformed by an external force, it can return to the pre-deformed shape by heating. SMAs have shape memory effect and superelasticity, as well as good physical and chemical properties and biocompatibility [1]. As the actuators based on SMA have the advantages of simple structure, small size, light quality, and low cost, the SMA is increasingly used in different fields [2]. For example, advanced SMA-based devices have been designed to improve the aerodynamic performance of vehicles [3], to actuate light grippers and reusable non-explosive lock release mechanisms [4,5], and to generate constant force components [6], etc.

However, how to accurately and effectively control the output force and displacement of the SMA is challenging. The resistance characteristics of SMA is important for the closed-loop control of SMA actuators. When displacement or force is used as the feedback signal in the control of the SMA, it is necessary to add a corresponding displacement sensor or force sensor. However, in practical engineering applications, the addition of external sensors will increase the volume of the structure

and the whole process of detecting the state of the SMA cannot be realized effectively. Therefore, as an internal variable of SMA, the resistance can be considered as a feedback signal in the control. The resistance changes with the state of SMA in real time, and the measurement circuit can be quite small, which is more conducive to the practical application of SMA actuators [7]. In order to make the resistance of SMA an effective feedback variable, it is first necessary to establish the relationship between resistance and strain. The research on the resistance characteristics of SMA is usually based on the constitutive model of SMA and combined with the resistance law [8].

Furst et al. studied a single-shape memory alloy spring system by adding a second opposing shape memory alloy wire and focusing on the resistance to strain mapping that is crucial for self-sensing applications [9]. Zhu et al. applied this method to the self-repair of shape memory alloy composites to eliminate cracks and prevent overheating as soon as possible [10]. Nahm et al. studied the relationship between resistivity and tensile properties of Ni-Ti SMA wires for the process of superelasticity of SMA. The possibility of application of Ni-Ti SMA wire as a sensor was also studied. The sensor system can measure strain of 6%, and measurement error is 0.22%, and sensitivity of the rate of resistivity is 0.005% [11]. Yan et al. established a resistance–strain model of SMA for the process of superelasticity by using thermal dynamic and resistance theories. On the basis of this model, a piecewise linear model of the process of superelasticity was established through numerical analysis and experimental verification [12]. Cui et al. established a resistance characteristic model of Ni-Ti SMAs. The relationship between the change of the relative resistance and strain of SMA at different temperatures was analyzed, and the resistance characteristics of Ni-Ti SMA wires were tested to verify the validity of the model [13]. Also, Cui et al. analyzed the sensing principle based on the resistance of SMA. According to the relation between the resistivity of SMA wire and martensitic volume fraction, a mathematical model was established, which is applicable to different temperatures and initial conditions. The numerical simulation results based on the model are in good agreement with the experimental results, indicating that SMA wires with appropriate models can be used as sensing elements [14]. Xu et al. established the resistance characteristic model of Ni-Ti SMA fibers based on the mixed law of the martensite growth model and resistance. The relationship between resistivity and temperature of the fibers at zero stress was also studied [15]. Zhang et al. designed an embedded control circuit based on SMA internal resistance feedback. The heating control circuit of the SMA actuator and the resistance measurement and acquisition circuit of constant current source bridge method were built using an ATMEGA16 microcontroller. The experiment showed that the measurement method can achieve sufficient accuracy [16]. Lynch et al. proposed a stress–strain–resistance model. The model considers different loads, primary and secondary hysteresis effects, and is normalized according to the geometry of the actuator. The simulation results and a simple position control experiment were used to verify the performance of the model, and the correlation between the model and Liang’s enhancement model was proposed [17]. It can be seen that, in order to reflect the deformation of SMA via the change of resistance, many studies have been done on the resistance characteristic models of SMA [18,19]. The most common way to establish the resistance characteristic model is to use the constitutive model of SMA to reveal the relationship between resistance and strain [20]. Therefore, the accuracy of the constitutive model will directly determine the quality of the resistance model. For one-dimensional SMA actuators, the most commonly used constitutive model is the one-dimensional macro phenomenological constitutive model, because it introduces less internal variables and can easily predict the thermomechanical behaviors of SMA [21–23]. However, most of the existing resistance characteristic models are based on Liang’s model or Brinson’s model, which ignore the influence of the phase transformation rate distribution on the change of SMA’s resistivity [12–17]. Therefore, it is difficult to accurately predict the resistance characteristic of the SMA during the phase transformation process with a high degree of asymmetry.

In this paper, the resistance characteristic model of SMA is established from the perspective of the relative change of resistance, and the variable speed phase transformation constitutive model is used to acquire the parameters that affect the change of resistance. In this model, the effects of

the resistivity, length and cross-sectional area of SMA on the relative change of resistance are fully considered. In order to simulate the relationship between resistance and strain, the characteristic parameters of the Ni-Ti SMA wire were identified using experiments, including the DSC experiment, the loading experiment and the thermal cycling experiment. The Ni and Ti contents of the SMA wire were 54.94 wt % and 45.06 wt %, respectively. Finally, the simulation results were analyzed and the possibility of using resistance for feedback control was proved.

2. Variable Speed Phase Transformation Constitutive Model

The phase composition of SMA changes with its stress and temperature. When the stress increases above the start critical stress (σ_s), twinned martensite is transformed into detwinned martensite, and when the stress reaches the finish critical stress (σ_f), the transformation is complete. However, when the stress decreases, the phase composition does not change. When the temperature increases to the austenite start temperature (A_s), martensite (including twinned and detwinned martensite) is transformed into austenite, and when the temperature reaches the austenite finish temperature (A_f), the transformation is complete. When the temperature decreases to the martensite start temperature (M_s), the austenite is transformed into twinned martensite, and when the temperature reaches the martensite finish temperature (M_f), the transformation is complete. In this study, a new variable speed phase transformation model is used to describe the phase composition change of SMA, including the phase transformation equation and the constitutive equation.

2.1. Phase Transformation Equation

In all the thermomechanical behaviors of SMA, the crystal phase transformation process of SMAs can be divided into three categories: martensite (M) to austenite (A), austenite (A) to martensite (M), and twinned martensite (TM) to detwinned martensite (DM). By referring to the derivation process of Liang and introducing the crystal variable speed function K , a new constitutive model was obtained in our previous research [23]. For a specific phase transformation process of the SMA, the crystal variable function K can be determined by the material parameters of SMA and a crystal variable speed coefficient k . The coefficient k is a constant determined by experiments, which reflects the rate distribution of the volume fraction of martensite/austenite with temperature or stress during the transformation process. Please note that all the variables and abbreviations mentioned in this article and their meanings are shown in Appendix A.

For the $M \rightarrow A$ transformation process, the volume fraction of austenite can be derived as

$$\xi_A = 1 + (\xi_{A0} - 1) \left\{ \frac{1}{2} \left[\cos \frac{\pi(T - A_s - \sigma/C_A)}{(A_s - A_f)} + 1 \right] \right\}^{K_1} \quad (1)$$

where

$$K_1 = \left[1 - \frac{(T - A_s - \sigma/C_A)(k_1 - 1)}{(A_f - A_s)k_1} \right] k_1 \quad (2)$$

For the $A \rightarrow M$ transformation process, the volume fraction of austenite is derived as

$$\xi_A = \xi_{A0} \left\{ \frac{1}{2} \left[\cos \frac{\pi(T - M_s - \sigma/C_M)}{(M_s - M_f)} + 1 \right] \right\}^{K_2} \quad (3)$$

where

$$K_2 = \left[1 + \frac{(T - M_s - \sigma/C_M)(k_2 - 1)}{(M_s - M_f)k_2} \right] k_2 \quad (4)$$

where C_A and C_M are coefficients related to the phase transformation critical stress and the phase transformation temperature of SMAs.

For the $TM \rightarrow DM$ transformation process, the volume fraction of detwinned martensite is derived as

$$\xi_{DM} = 1 - \xi_A + (1 - \xi_A)(\xi_{DM0} - 1) \left\{ \frac{1}{2} \left[\cos \frac{\pi(\sigma - \sigma_s)}{(\sigma_s - \sigma_f)} + 1 \right] \right\}^{k_3} \quad (5)$$

where

$$K_3 = \left[1 - \frac{(\sigma - \sigma_s)(k_3 - 1)}{(\sigma_f - \sigma_s)k_3} \right] k_3 \quad (6)$$

2.2. Constitutive Equation

The total strain of the SMA can be divided into three parts: the strain induced by elasticity, the strain induced by phase transformation and the strain induced by thermo [24]. According to the above strain classification, the constitutive equation can be derived as

$$\varepsilon - \varepsilon_0 = \frac{\sigma}{E(\xi_A, \xi_{DM})} - \frac{\sigma_0}{E(\xi_{A0}, \xi_{DM0})} + \Psi(\xi_{DM} - \xi_{DM0}) + \alpha(\xi_A)T - \alpha(\xi_{A0})T_0 \quad (7)$$

where

$$E(\xi_A, \xi_{DM}) = E_{TM} + (E_A - E_{TM})\xi_A + (E_{DM} - E_{TM})\xi_{DM} \quad (8)$$

$$\alpha(\xi_A) = \alpha_M + (\alpha_A - \alpha_M)\xi_A \quad (9)$$

$$\Psi = \varepsilon_L \quad (10)$$

The volume fraction of each crystal phase in the transformation process was derived in Section 2.1. A numerical simulation of the constitutive model was performed with the initial state setting as $\varepsilon_0 = 0$, $\sigma_0 = 0$, $\xi_{TM0} = 1$, $T_0 = 0$ °C. The results are presented in Figure 1, which reveals the relationship between temperature, stress, and strain of the SMA. The parameters used in the simulation can be found in Tables 1 and 2, which are identified by experiment.

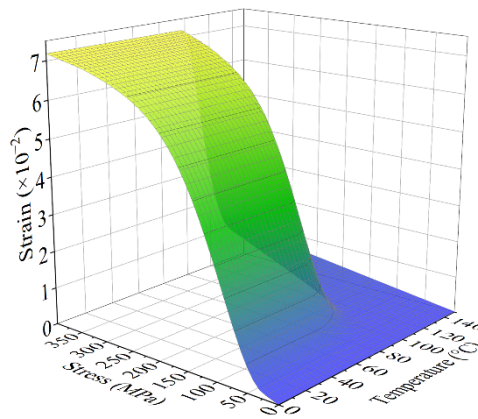


Figure 1. Relationship between temperature, stress, and strain of the shape memory alloy (SMA).

Table 1. Thermal and mechanical parameters of the SMA.

M_f (°C)	M_s (°C)	A_s (°C)	A_f (°C)	σ_s (MPa)	σ_f (MPa)
35.8	62.8	47.6	81.9	26.5	326.8
E_A (GPa)	E_{TM} (GPa)	E_{DM} (GPa)	C_M (MPa/°C)	C_A (MPa/°C)	ε_L
54.64	17.96	31.52	10.4	8.0	0.0645
α_M (°C ⁻¹)	α_A (°C ⁻¹)	l_0 (mm)	k_1	k_2	k_3
2.73×10^{-7}	9.16×10^{-7}	100	1.15	1.28	7.88

Table 2. Electrical parameters of the SMA.

ν	a ($^{\circ}\text{C}^{-1}$)	ρ_{TM} ($\Omega\cdot\text{m}$)	ρ_{DM} ($\Omega\cdot\text{m}$)	ρ_A ($\Omega\cdot\text{m}$)
0.3	8.75×10^{-4}	0.87×10^{-6}	0.82×10^{-6}	0.72×10^{-6}

With the above-mentioned constitutive model, the resistance characteristic model of SMA will be derived in the next section, which can predict the thermomechanical behaviors of SMA in accordance with its resistance.

3. Resistance Characteristic Model

In this part, a one-dimension SMA wire is considered. The resistance R of the SMA can be described as

$$R = \frac{\rho l}{S} \quad (11)$$

where ρ is the resistivity, l is the length, and S is the cross-sectional area. By taking the natural logarithm of Equation (11), and then applying the total differential operator, the resistance equation can be derived as

$$\frac{dR}{R} = \frac{d\rho}{\rho} + \frac{dl}{l} - \frac{dS}{S} \quad (12)$$

Thus, the three factors affecting the change of resistance of SMA are separated and can be expressed separately. Among them, the resistivity varies with temperature, which can be described as

$$\rho = \rho_0(1 + aT) \quad (13)$$

where ρ_0 is the resistivity when temperature is 0°C , and a is the temperature coefficient of resistance. Therefore, the resistivity equation of the decomposed form can be obtained as

$$\frac{d\rho}{\rho} = \frac{d\rho_0}{\rho_0} + \frac{adT}{1 + aT} \quad (14)$$

Since ρ_0 is affected by the volume fraction of twinned martensite, detwinned martensite and austenite, ρ_0 can be described as

$$\rho_0 = \rho_{TM} + (\rho_A - \rho_{TM})\xi_A + (\rho_{DM} - \rho_{TM})\xi_{DM} \quad (15)$$

where ρ_{TM} is the resistivity of twinned martensite, ρ_{DM} is the resistivity of detwinned martensite, and ρ_A is the resistivity of austenite. Since both ξ_A and ξ_{DM} are functions of temperature and stress, ρ_0 is the function of temperature T and stress σ , too. Combining with the phase transformation equation of the constitutive model from Equations (1)–(6), the relation between ρ_0 , T and σ can be obtained. A numerical simulation of the resistivity of SMA was carried out. The relationship between temperature, stress, and resistivity of the SMA is shown in Figure 2. The parameters used in the simulation are collected in Tables 1 and 2.

Substituting Equations (14) into Equations (12), the resistance equation is derived as

$$\frac{dR}{R} = \frac{d\rho_0}{\rho_0} + \frac{adT}{1 + aT} + \frac{dl}{l} - \frac{dS}{S} \quad (16)$$

where

$$\frac{dS}{S} = \frac{2\pi r dr}{\pi r^2} = 2 \frac{dr}{r} = -2\nu \frac{dl}{l} \quad (17)$$

where r is the radius of the cross section, and ν is Poisson's ratio. Convert Equation (16) into incremental form, the resistance characteristic model can be finally derived as

$$\frac{\Delta R}{R} = \frac{\Delta \rho_0}{\rho_0} + \frac{a \Delta T}{1 + aT} + (1 + 2\nu)\varepsilon \quad (18)$$

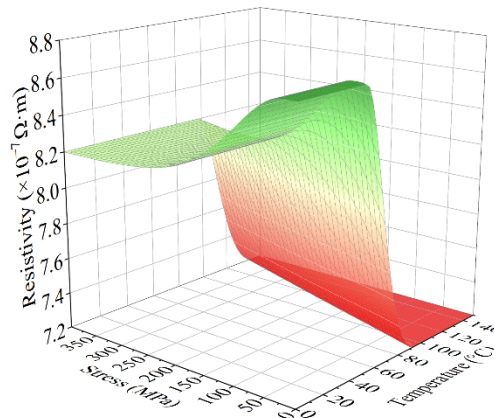
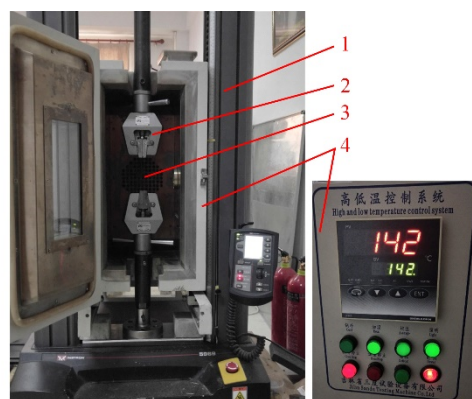


Figure 2. Relationship between temperature, stress and resistivity of the SMA.

4. Parameter Identification

The parameters of the SMA wire are identified by experiments. The diameter of the SMA wire is 0.4 mm, with 54.94 wt % Ni and 45.06 wt % Ti. Firstly, the DSC experiment using a DSC synchronous thermal analyzer (LINSEIS STA PT1000) was performed, which gave the phase transformation temperatures, and the coefficients k_1 and k_2 . Then, the loading experiments at 25 and 100 °C were performed with a tensile testing machine and a miniature high-low temperature chamber, as shown in Figure 3. The elastic moduli, critical stresses, maximum residual strain and the coefficient k_3 were obtained. Finally, the thermal cycling experiment was conducted using a high-low temperature chamber (GDW/GDJS-100) and a laser displacement sensor (Keyence LK-G5000), as shown in Figure 4, based on which the coefficient C_A as well as C_M were obtained. The thermal and mechanical parameters of the SMA wire are collected in Table 1. The electrical parameters of the SMA were measured by an Agilent digital multimeter (344450A) and listed in Table 2.



1. Tensile testing machine 2. Clamping fixtures 3. SMA wire
4. Miniature high-low temperature chamber

Figure 3. The loading experiments at 25 °C and 100 °C.

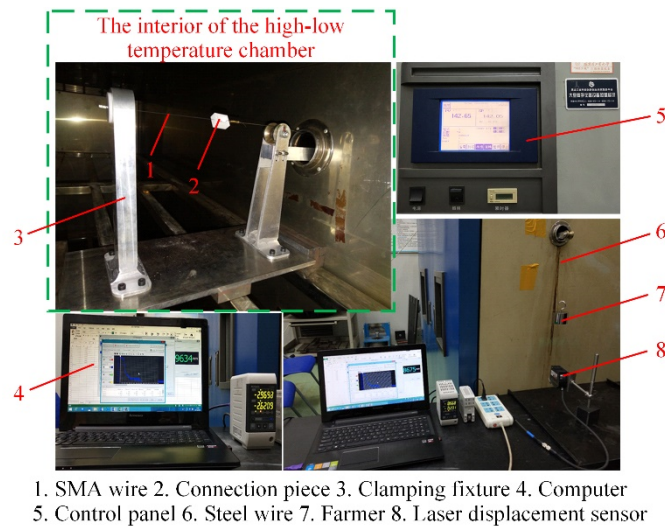


Figure 4. The thermal cycling experiments.

5. Numerical Simulation

Numerical simulations of three cases were carried out: the loading experiments at 25 °C (100% martensite in the SMA), the loading experiments at 100 °C (100% austenite in the SMA), and the thermal cycling experiment. The parameters used in the numerical simulation are shown in Tables 1 and 2. The initial condition of loading at 25 °C is $\epsilon_0 = 0, \sigma_0 = 0, \rho_0 = \rho_{TM}$. Assuming that the temperature is constant during the experiment, the relative change in resistance in this case is

$$\frac{\Delta R}{R_r} = \frac{\Delta \rho_0}{\rho_{TM}} + (1 + 2\nu)\epsilon \tag{19}$$

where $\Delta \rho_0 = \rho_0 - \rho_{TM}$. Combined with the variable speed phase transformation constitutive model, the three-segment function of the loading process is

$$\frac{\Delta R}{R_r} = \begin{cases} (1 + 2\nu)\frac{\sigma}{E_{TM}}, & \sigma < \sigma_s \\ \frac{\rho_{DM} - \rho_{TM}}{\rho_{TM}} \xi_{DM} + (1 + 2\nu)\left(\frac{\sigma}{E(\xi_A, \xi_{DM})} + \Psi \xi_{DM}\right), & \sigma_s \leq \sigma < \sigma_f \\ \frac{\rho_{DM} - \rho_{TM}}{\rho_{TM}} + (1 + 2\nu)\left(\frac{\sigma}{E_{DM}} + \epsilon_L\right), & \sigma \geq \sigma_f \end{cases} \tag{20}$$

The function of the unloading process is

$$\frac{\Delta R}{R_r} = \frac{\rho_{DM} - \rho_{TM}}{\rho_{TM}} + (1 + 2\nu)\left(\frac{\sigma}{E_{DM}} + \epsilon_L\right) \tag{21}$$

where $\xi_{DM}, E(\xi_A, \xi_{DM})$, and Ψ are obtained from Section 2. The relative change of resistance $\Delta R/R_r$ can be simulated by MATLAB. Combined with the simulation results of strain ϵ , the relations between $\Delta R/R_r$ and ϵ are plotted in Figure 5.

The initial condition of loading at 100 °C is $\epsilon_0 = \alpha_A T_0 - \alpha_M T_r, \sigma_0 = 0, \rho_0 = \rho_A$. Assuming that the temperature is constant during the experiment, the relative change in resistance in this case is

$$\frac{\Delta R}{R_r} = \frac{\Delta \rho_0}{\rho_{TM}} + (1 + 2\nu)(\epsilon - \epsilon_0) \tag{22}$$

where $\Delta \rho_0 = \rho_0 - \rho_A = \rho_{TM} + (\rho_A - \rho_{TM})\xi_A + (\rho_{DM} - \rho_{TM})\xi_{DM} - \rho_A$. Combined with the variable speed phase transformation constitutive model, the three-segment function of the loading process is

$$\frac{\Delta R}{R_r} = \begin{cases} (1 + 2\nu) \frac{\sigma}{E_A}, & \sigma < C_M(T - M_{s0}) \\ \frac{\Delta \rho_0}{\rho_{TM}} + (1 + 2\nu)\Delta \varepsilon, & C_M(T - M_{s0}) \leq \sigma < C_M(T - M_{f0}) \\ \frac{\rho_{DM} - \rho_A}{\rho_{TM}} + (1 + 2\nu) \left(\frac{\sigma}{E_{DM}} + \Psi + \alpha_M T_0 - \alpha_A T_0 \right), & \sigma \geq C_M(T - M_{f0}) \end{cases} \quad (23)$$

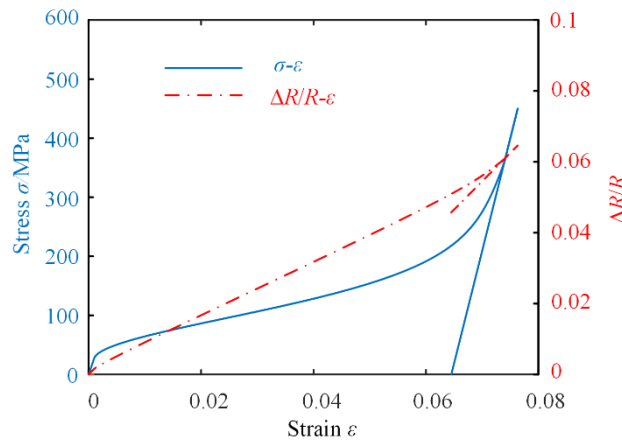


Figure 5. The relationship between σ - ε and σ - $\Delta R/R$ at 25 °C.

The three-segment function of the unloading process is

$$\frac{\Delta R}{R_r} = \begin{cases} \frac{\rho_{DM} - \rho_A}{\rho_{TM}} + (1 + 2\nu) \left(\frac{\sigma}{E_{DM}} + \Psi + \alpha_M T_0 - \alpha_A T_0 \right), & \sigma \geq C_A(T - A_{s0}) \\ \frac{\Delta \rho_0}{\rho_{TM}} + (1 + 2\nu)\Delta \varepsilon, & C_A(T - A_{f0}) \leq \sigma < C_A(T - A_{s0}) \\ (1 + 2\nu) \frac{\sigma}{E_A}, & \sigma < C_A(T - A_{f0}) \end{cases} \quad (24)$$

where

$$\Delta \varepsilon = \frac{\sigma}{E(\xi_A, \xi_{DM})} + \Psi \xi_{DM} + \alpha(\xi_A) T_0 - \alpha_A T_0 \quad (25)$$

where ξ_A , ξ_{DM} , $E(\xi_A, \xi_{DM})$, $\alpha(\xi_A)$, and Ψ are obtained from Section 2. The relative change in resistance $\Delta R/R_r$ can be simulated by MATLAB. Combined with the simulation results of strain ε , the relations between $\Delta R/R_r$ and ε are presented in Figure 6.

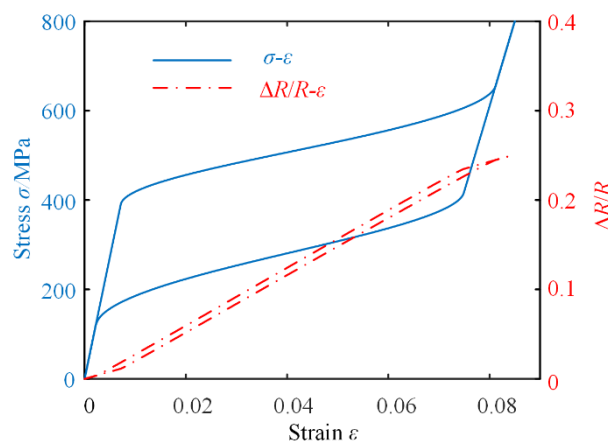


Figure 6. The relationship between σ - ε and σ - $\Delta R/R$ at 100 °C.

The initial condition of the thermal cycling experiment is $\sigma_0 = 117 \text{ MPa}$, $T_0 = 25 \text{ }^\circ\text{C}$ ($T_0 < M_{f0}$), $\xi_{A0} = 0$. Combining constitutive Equation (7) with phase transformation Equation (5), ε_0 is

$$\varepsilon_0 = \frac{\sigma_0}{E(\xi_{A0}, \xi_{DM0})} + \Psi \xi_{DM0} \tag{26}$$

$$\xi_{DM0} = 1 - \left\{ \frac{1}{2} \left[\cos \frac{\pi(\sigma_0 - \sigma_s)}{(\sigma_s - \sigma_f)} + 1 \right] \right\}^{K_3} \tag{27}$$

The stress changed little during the whole experiment, so it can be assumed that the stress was constant. The relative change of resistance is

$$\frac{\Delta R}{R_r} = \frac{\Delta \rho_0}{\rho_{TM}} + \frac{a \Delta T}{1 + a T_0} + (1 + 2\nu)(\varepsilon - \varepsilon_0) \tag{28}$$

where $\Delta \rho_0 = \rho_0 - \rho_{00} = (\rho_A - \rho_{TM})(\xi_A - \xi_{A0}) + (\rho_{DM} - \rho_{TM})(\xi_{DM} - \xi_{DM0})$.

Combined with the variable speed phase transformation constitutive model, the three-segment function of the heating process is

$$\frac{\Delta R}{R_r} = \begin{cases} \frac{a(T-T_0)}{1+aT_0} + (1+2\nu)\alpha_M(T-T_0), & T_0 < T < \frac{\sigma_0}{C_A} + A_s \\ \frac{\Delta \rho_0}{\rho_{TM}} + \frac{a(T-T_0)}{1+aT_0} + (1+2\nu)\Delta \varepsilon_1, & \frac{\sigma_0}{C_A} + A_s \leq T < \frac{\sigma_0}{C_A} + A_f \\ \frac{\Delta \rho_0}{\rho_{TM}} + \frac{a(T-T_0)}{1+aT_0} + (1+2\nu)\Delta \varepsilon_2, & T \geq \frac{\sigma_0}{C_A} + A_f \end{cases} \tag{29}$$

The three-segment function of the cooling process is

$$\frac{\Delta R}{R_r} = \begin{cases} \frac{\Delta \rho_0}{\rho_{TM}} + \frac{a(T-T_0)}{1+aT_0} + (1+2\nu)\Delta \varepsilon_2, & T \geq \frac{\sigma_0}{C_M} + M_s \\ \frac{\Delta \rho_0}{\rho_{TM}} + \frac{a(T-T_0)}{1+aT_0} + (1+2\nu)\Delta \varepsilon_1, & \frac{\sigma_0}{C_M} + M_f \leq T < \frac{\sigma_0}{C_M} + M_s \\ \frac{a(T-T_0)}{1+aT_0} + (1+2\nu)\alpha_M(T-T_0), & T_0 < T < \frac{\sigma_0}{C_M} + M_f \end{cases} \tag{30}$$

where

$$\Delta \varepsilon_1 = \frac{\sigma_0}{E(\xi_A, \xi_{DM})} - \frac{\sigma_0}{E(\xi_{A0}, \xi_{DM0})} + \Psi(\xi_{DM} - \xi_{DM0}) + \alpha(\xi_A)T - \alpha_M T_0 \tag{31}$$

$$\Delta \varepsilon_2 = \frac{\sigma_0}{E_A} - \frac{\sigma_0}{E(\xi_{A0}, \xi_{DM0})} - \Psi \xi_{DM0} + \alpha_A T - \alpha_M T_0 \tag{32}$$

where ξ_A , ξ_{DM} , $E(\xi_A, \xi_{DM})$, $E(\xi_{A0}, \xi_{DM0})$, $\alpha(\xi_A)$, and Ψ are obtained from Section 2. The relative change in resistance $\Delta R/R_r$ can be simulated by MATLAB. Combined with the simulation results of strain ε , the relations between $\Delta R/R_r$ and ε are depicted in Figure 7.

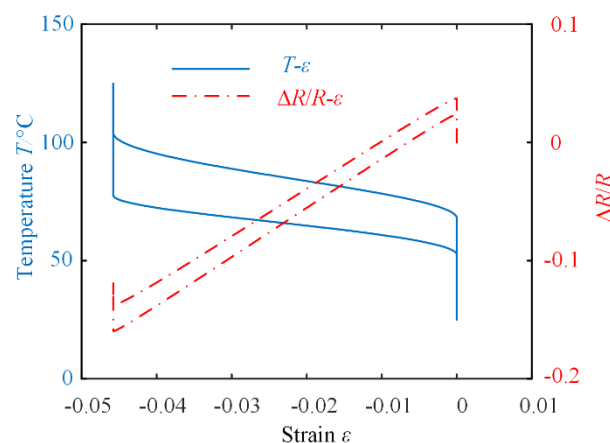


Figure 7. The relationship between $T-\varepsilon$ and $\sigma-\Delta R/R$ at 117 MPa.

It can be observed from Figure 5 to Figure 7 that for different cases, the relative change in resistance of the SMA varies corresponding to the strain. In fact, for most applications of SMA-based actuators, we just need to pay close attention to a particular phase transition process of the SMA. Thus, it is possible to monitor the resistance instead of the strain of the SMA for precision control of the SMA-based actuator. The proposed SMA resistance characteristic model can therefore be used to accurately calculate the output displacement or force of the actuator.

6. Conclusions

A new resistance characteristic model of SMA was proposed in this work based on the variable speed phase transformation constitutive model. The influences of different parameters, such as the resistivity, the length, the cross-sectional area of the SMA, and the temperature on the resistance, were fully considered. The coupling relationship of stress–strain–temperature–resistance of SMA was revealed. Compared with the existing models, the proposed model further considers the influence of the phase transformation rate on the change of SMA's resistivity, which can greatly enhance the accuracy of the model, especially for those with distinct asymmetry phase transformation process. Therefore, the proposed model can describe the one-to-one correspondence between resistance and strain of SMA in a particular phase transformation process more accurately and comprehensively; namely, the resistance can be used as an internal variable to reflect the strain of SMA. The model serves as an important theoretical basis for precision control of SMA-based actuator with resistance signal feedback, which will further promote the study on the control of SMA-based systems, and is conducive to the lightweight and miniaturization of SMA-based structures.

Author Contributions: Conceptualization, Y.L. and R.Z.; Investigation, L.W.; Methodology, Y.X.; Project administration, H.Y.; Writing—original draft, Y.L.; Writing—review & editing, Y.L. All authors have read and agreed to the published version of the manuscript.

Funding: This research is funded by Self-Planned Task of State Key Laboratory of Robotics and System (Grant No. SKLRS201808B), China Postdoctoral Science Foundation (Grant No. 2019M661289), and National Natural Science Foundation of China (Grant No. 51875115).

Conflicts of Interest: The authors declare no conflict of interest.

Appendix A

Table A1. Nomenclature.

Symbol	Meaning	Symbol	Meaning
T	Temperature	k	Crystal variable speed coefficient
M_s	Martensite start temperature	K	Crystal variable speed function
M_f	Martensite finish temperature	A	Austenite
A_s	Austenite start temperature	DM	Detwinned martensite
A_f	Austenite finish temperature	TM	Twinned martensite
M_p	Martensite peak temperature	Ψ	Transformation modulus
A_p	Austenite peak temperature	E_A	Elastic modulus of austenite
σ	Stress	E_{TM}	Elastic modulus of TM
σ_s	Starting stress	E_{DM}	Elastic modulus of DM
σ_f	Finishing stress	ξ_A	Volume fraction of austenite
σ_p	Peaking stress	ξ_{DM}	Volume fraction of DM
ε	Strain	ε_L	Maximum residual strain
α_M	Thermal expansion coefficient of martensite	α_A	Thermal expansion coefficient of austenite
ν	Poisson's ratio	a	Temperature coefficient of R
S	Cross-sectional area.	l	Length
ρ	Resistivity	ρ_{TM}	Resistivity of TM
P_{DM}	Resistivity DM	ρ_A	Resistivity DM

References

- Hartl, D.J.; Lagoudas, D.C. Aerospace applications of shape memory alloys. *Proc. Inst. Mech. Eng. Part G: J. Aerosp. Eng.* **2007**, *221*, 535–552. [CrossRef]

2. Jani, J.M.; Leary, M.; Subic, A.; Gibson, M.A. A review of shape memory alloy research, applications and opportunities. *Mater. Des.* **2014**, *56*, 1078–1113. [[CrossRef](#)]
3. Sellitto, A.; Riccio, A. Overview and Future Advanced Engineering Applications for Morphing Surfaces by Shape Memory Alloy Materials. *Materials* **2019**, *12*, 708. [[CrossRef](#)] [[PubMed](#)]
4. Lu, Y.; Xie, Z.; Wang, J.; Yue, H.; Wu, M.; Liu, Y. A novel design of a parallel gripper actuated by a large-stroke shape memory alloy actuator. *Int. J. Mech. Sci.* **2019**, *159*, 74–80. [[CrossRef](#)]
5. Pan, X.; Zhang, Y.; Lu, Y.; Yang, F.; Yue, H. A reusable SMA actuated non-explosive lock-release mechanism for space application. *Int. J. Smart Nano Mater.* **2020**, 1–13. [[CrossRef](#)]
6. Wang, M.; Yu, H.; Shi, P.; Meng, Q. Design Method for Constant Force Components Based on Superelastic SMA. *Materials* **2019**, *12*, 2842. [[CrossRef](#)]
7. Dhanalakshmi, K. Differential resistance feedback control of a self-sensing shape memory alloy actuated system. *ISA Trans.* **2014**, *53*, 289–297. [[CrossRef](#)]
8. Furst, S.J.; Seelecke, S. Modeling and experimental characterization of the stress, strain, and resistance of shape memory alloy actuator wires with controlled power input. *J. Intell. Mater. Syst. Struct.* **2012**, *23*, 1233–1247. [[CrossRef](#)]
9. Furst, S.J.; Crews, J.H.; Seelecke, S. Stress, strain, and resistance behavior of two opposing shape memory alloy actuator wires for resistance-based self-sensing applications. *J. Intell. Mater. Syst. Struct.* **2013**, *24*, 1951–1968. [[CrossRef](#)]
10. Zhu, Y.T.; Hagiwara, I.; Yasuhiro, M. Research on sensing and control of shape memory alloy embedded in intelligent material. *Chin. J. Mech. Eng.* **2005**, *41*, 221–225. [[CrossRef](#)]
11. Nahm, S.H.; Kim, Y.J.; Kim, J.M.; Yoon, D.J. A study on the application of Ni-Ti shape memory alloy as a sensor. *Mater. Sci. Forum* **2005**, *475*, 2043–2046. [[CrossRef](#)]
12. Yan, S.; Zhang, Y.; Wang, W.; Yu, Z. Electrical Resistance-Strain Model for Shape Memory Alloys. *J. Shenyang Jianzhu Univ. Nat. Sci.* **2008**, *24*, 980–984.
13. Cui, D.; Li, H.; Song, G. Study on electrical resistance properties of shape memory alloy. *J. Build. Mater.* **2008**, *11*, 567–573.
14. Cui, D.; Song, G.; Li, H. Modeling of the electrical resistance of shape memory alloy wires. *Smart Mater. Struct.* **2010**, *19*, 055019. [[CrossRef](#)]
15. Xu, L.; Wang, R.; Zhang, S. Electrical resistance properties of Ni-Ti shape memory alloy fiber in phase transformation. *J. Text. Res.* **2010**, *31*, 15–19.
16. Zhang, J.; Chen, B.; Geng, L.; Chen, S.; Wu, H. Design of control system for SMA actuator based on resistance feedback. *Microprocessors* **2011**, *35*, 91–93.
17. Lynch, B.; Jiang, X.X.; Ellery, A.; Nitzsche, F. Characterization, modeling, and control of Ni-Ti shape memory alloy based on electrical resistance feedback. *J. Intell. Mater. Syst. Struct.* **2016**, *27*, 2489–2507. [[CrossRef](#)]
18. Brinson, L.C.; Huang, M.S. Simplifications and comparisons of shape memory alloy constitutive models. *J. Intell. Mater. Syst. Struct.* **1996**, *7*, 108–114. [[CrossRef](#)]
19. Liang, C.; Rogers, C.A. One-dimensional thermomechanical constitutive relations for shape memory materials. *J. Intell. Mater. Syst. Struct.* **1997**, *8*, 285–302. [[CrossRef](#)]
20. Cisse, C.; Zaki, W.; Zineb, T.B. A review of constitutive models and modeling techniques for shape memory alloys. *Int. J. Plast.* **2016**, *76*, 244–284. [[CrossRef](#)]
21. Zhou, B.; Yoon, S.H.; Leng, J.S. A three-dimensional constitutive model for shape memory alloy. *Smart Mater. Struct.* **2009**, *18*, 095016. [[CrossRef](#)]
22. Zhou, B.; Yoon, S.H. A new phase transformation constitutive model of shape memory alloys. *Smart Mater. Struct.* **2006**, *15*, 1967–1973. [[CrossRef](#)]
23. Lu, Y.; Zhang, R.; Xie, Z.; Yue, H.; Wang, L. A new variable speed phase transformation constitutive model of shape memory alloys. *Mater. Res. Express* **2019**, *6*, 105705. [[CrossRef](#)]
24. Lagoudas, D.C. *Shape Memory Alloys: Modeling and Engineering Applications*; Springer Science & Business Media: New York, NY, USA, 2008. [[CrossRef](#)]



© 2020 by the authors. Licensee MDPI, Basel, Switzerland. This article is an open access article distributed under the terms and conditions of the Creative Commons Attribution (CC BY) license (<http://creativecommons.org/licenses/by/4.0/>).

© 2020. This work is licensed under <http://creativecommons.org/licenses/by/3.0/> (the “License”). Notwithstanding the ProQuest Terms and Conditions, you may use this content in accordance with the terms of the License.